Published in final edited form as:
Clin Cancer Res. 2020 April 01; 26(7): 1700–1711. doi:10.1158/1078-0432.CCR-19-2202.

Preclinical evaluation of a novel SHIP1 phosphatase activator for inhibition of PI3K signaling in malignant B-cells

Elizabeth Lemm[#1], **Beatriz Valle-Argos**[#1], **Lindsay D. Smith**[1], **Johanna Richter**[1], **Yohannes Gebreselassie**[1], **Matthew Carter**[2], **Jana Karolova**[3,4], **Michael Svaton**[3,4], **Karel Helman**[5], **Nicola Weston-Bell**[1], **Laura I Karydis**[1], **Chris T Williamson**[6], **Georg Lenz**[7], **Jeremy D Pettigrew**[6], **Curtis Harwig**[6], **Freda K Stevenson**[1], **Mark S Cragg**[1], **Francesco Forconi**[1], **Andrew J Steele**[1], **Jennifer L Cross**[6], **Lloyd F Mackenzie**[6], **Pavel Klener**[3,4], **Graham Packham**[1]

[1]Cancer Research UK Centre, Cancer Sciences Unit, Faculty of Medicine, University of Southampton, Southampton, United Kingdom

[2]Centre for Cancer Immunology, Cancer Sciences Unit, Faculty of Medicine, University of Southampton, Southampton, United Kingdom

[3]Institute of Pathological Physiology, First Faculty of Medicine, Charles University, Prague, Czech Republic

[4]CLIP – Childhood Leukaemia Investigation Prague, Second Faculty of Medicine and Charles University Hospital in Motol, Prague, Czech Republic

[5]Faculty of Informatics and Statistics, University of Economics, Prague, Czech Republic

[6]Aquinox Pharmaceuticals (Canada) Inc., Vancouver, British Columbia, Canada

[7]Department of Medicine A for Hematology, Oncology, and Pneumology, University Hospital Munster, Munster, Germany

[#] These authors contributed equally to this work.

Abstract

Purpose—Phosphatidylinositol-3 kinase (PI3K) signaling is a common feature of B-cell neoplasms, including chronic lymphocytic leukemia (CLL) and diffuse large B-cell lymphoma (DLBCL), and PI3K inhibitors have been introduced into the clinic. However, there remains a clear need to develop new strategies to target PI3K signaling. PI3K activity is countered by Src

Correspondence. Professor Graham Packham, Cancer Research UK Centre, Somers Research Building, Southampton General Hospital, Southampton, SO16 6YD. United Kingdom. gpackham@soton.ac.uk.

Contributions

EL, BVA, LS, JR, YG, MC, NW-B, LIK, JP, CH, KH, JK and MS performed experiments and analyzed results. CTW, MSC, GL, FKS, MSC, FF, AJS, JLC, LFM, PK and GP designed the research strategy, overall experimental plan and analyzed results. GP wrote the original draft of the manuscript and all authors contributed to its revision.

Conflict-of-interest disclosure. GP and PK received research funding from Aquinox Pharmaceuticals (Canada) Inc. GP and MSC received research funding from Gilead Sciences Inc. GP received consultancy payments from Aquinox Pharmaceuticals (Canada) Inc. AJS received research funding from Janssen and Portola Pharmaceuticals and received consultancy payments from Portola Pharmaceuticals. AJS holds stock in Portola Pharmaceuticals. CH, JP, JLC, LFM, CW were employees of Aquinox Pharmaceuticals (Canada) Inc. at the time of the study and hold stock in Aquinox Pharmaceuticals (Canada) Inc.

Europe PMC Funders Author Manuscripts

homology domain 2-containing inositol-5'-phosphatase 1 (SHIP1) and, here, we have characterized the activity of a novel SHIP1 activator, AQX-435, in pre-clinical models of B-cell malignancies.

Experimental design—*In vitro* activity of AQX-435 was evaluated using primary CLL cells and DLBCL-derived cell lines. *In vivo* activity of AQX-435, alone or in combination with the BTK inhibitor ibrutinib, was assessed using DLBCL cell line and patient-derived xenograft models.

Results—Pharmacological activation of SHIP1 using AQX-435 was sufficient to inhibit anti-IgM-induced PI3K-mediated signaling, including induction of AKT phosphorylation and MYC expression, without effects on upstream SYK phosphorylation. AQX-435 also co-operated with the BTK inhibitor ibrutinib to enhance inhibition of anti-IgM-induced AKT phosphorylation. AQX-435 induced caspase-dependent apoptosis of CLL cells preferentially as compared to normal B cells, and overcame *in vitro* survival promoting effects of microenvironmental stimuli. Finally, AQX-435 reduced AKT phosphorylation and growth of DLBCL *in vivo*, and co-operated with ibrutinib for tumor growth inhibition.

Conclusions—Our results using AQX-435 demonstrate that SHIP1 activation may be an effective novel therapeutic strategy for treatment of B-cell neoplasms, alone or in combination with ibrutinib.

Keywords

PI3K; phosphatase; lymphoma; leukemia; B-cell receptor

Introduction

Phosphatidylinositol-3-kinases (PI3K) are key drivers of survival and growth of normal B cells (1). PI3K catalyze the phosphorylation of phosphatidylinositol-4,5-bisphosphate ($PI(4,5)P_2$) to generate phosphatidylinositol-3,4,5-triphosphate ($PI(3,4,5)P_3$) which serves as a docking site at the plasma membrane for various pleckstrin homology domain-containing proteins, including phospholipase Cγ2 (PLCγ2), Bruton's tyrosine kinase (BTK) and AKR mouse thymoma kinase (AKT). Once recruited, these effectors become fully activated and drive downstream signaling leading to cell growth and survival.

PI3K activity is countered by the phosphatases phosphatase and tensin homolog (PTEN) and Src homology domain 2-containing inositol-5'-phosphatase (SHIP)1/2. Whereas PTEN directly reverses PI3K activity to generate $PI(4,5)P_2$, SHIP1/2 catalyze conversion of $PI(3,4,5)P_3$ to phosphatidylinositol-3,4-bisphosphate ($PI(3,4)P_2$) (2). $PI(3,4)P_2$ has second messenger activity but, in contrast to $PI(3,4,5)P_3$, appears to act predominantly to suppress signaling (3). In addition to their catalytic functions, SHIP1/2 may also modulate signaling by acting as scaffold proteins (2).

Multiple signaling pathways converge on PI3Ks in various subtypes of B-cell neoplasms, including signaling downstream of the B-cell receptor (BCR), a major driver and therapeutic target for malignant B-cells (4). For example, PI3K is activated in diffuse large B-cell lymphoma (DLBCL) cells due to chronic or tonic BCR signaling (5), and, in chronic

lymphocytic leukemia (CLL) and follicular lymphoma (FL) cells, following engagement of the BCR by (auto)antigen or environmental lectins, respectively (6–8). In CLL, BCR signaling capacity (including activation of PI3K) is most strongly retained in samples with unmutated *IGHV* genes (U-CLL) compared to samples with mutated *IGHV* genes (M-CLL) and associates with poor patient outcomes (9,10). PI3K is also activated in malignant B cells downstream of other receptors, including chemokine receptors (11,12). Finally, expression of PTEN is frequently down-regulated through a variety of mechanisms in GCB-DLBCL (13).

The frequent activation of the PI3K pathway in B-cell neoplasms has led to the clinical development of PI3K inhibitors (PI3Ki). The PI3Kδ isoform-specific inhibitor idelalisib is approved for treatment of CLL, FL and small lymphocytic lymphoma (14). Although idelalisib can be highly effective, its use is limited by substantial toxicity, especially in the frontline setting (15,16). Moreover, idelalisib is relatively ineffective as a monotherapy in DLBCL. This lack of effectiveness appears to be due to activation of additional PI3K isoforms since dual inhibition of PI3Kα and δ is associated with increased cytotoxicity of DLBCL cell lines compared to PI3Kδ inhibition alone (2,17). Responses can be enhanced using more broadly acting PI3Ki, such as the PI3Kδ/γ inhibitor duvelisib and the PI3Kα/δ inhibitor copanlisib, or by combinations of idelalisib with other targeted agents, including the BTK inhibitor, ibrutinb (17–21). However, there remains a clear need for novel strategies to target PI3K signaling, ideally combining broad activity against multiple subtypes of B-cell neoplasms with low toxicity, and with potential for effective combination with other targeted agents.

Here, we have investigated the effects of pharmacological activation of SHIP1 as a novel strategy for inhibition of BCR-induced PI3K signaling in malignant B-cells. BCR stimulation results in activation of SHIP1 as part of a negative feedback response to limit signaling (22,23). Thus, deletion of *Inppd5* (encoding Ship1) in mouse B cells results in hyperactive BCR signaling (24). Enhanced BCR signaling in Ship1-deficient animals appears to be a consequence of both increased $PI(3,4)P_2$ and reduced accumulation of $PI(3,4,5)P_3$ since functional inactivation of *Plekha1* and *Plekha2*, which encode effectors that bind the SHIP1 product $PI(3,4)P_2$, has a similar phenotype to deletion of *Inppd5* (3). Activation of SHIP1 following BCR stimulation is mediated by induced phosphorylation and recruitment to the plasma membrane. This includes SYK-dependent phosphorylation of SHIP1 at Y^{1022} which then mediates binding to the BCR via the Dok-3 adaptor protein (2,23,25–27). Importantly, SHIP1 is amenable to pharmacological activation using chemical agonists (28). For example, AQX-MN100, a synthetic derivative of the natural product SHIP1 activator pelorol, induces allosteric activation of SHIP1 by binding to the C2 domain of SHIP1 (which lies adjacent to the C-terminal side of the catalytic site), and reduces AKT phosphorylation and induces apoptosis in multiple myeloma cell lines (29–31). However, the utility of pelorol and MN-100 is restricted by their extremely limited aqueous solubility (30). Moreover, effects of SHIP1 agonists specifically on BCR signalling and on the *in vivo* growth of neoplastic B cells have not been studied.

In this study we used a novel small molecule SHIP1 agonist, AQX-435, to investigate the effect of SHIP1 activation in preclinical models of B-cell neoplasms. AQX-435 was selected

from a panel of new pelorol-related compounds, synthesized to improve the aqueous solubility and other drug-like properties of this class of agonist (32). We focused on CLL and DLBCL, both of which are characterized by PI3K activation, and demonstrated that AQX-435 reduces PI3K activation downstream of the BCR and induces apoptosis of malignant B cells *in vitro*, and reduces lymphoma growth *in vivo*, alone or in combination with ibrutinib. Overall, our results demonstrate that SHIP1 activation is a potential new therapeutic approach for B-cell neoplasms and can be combined effectively with ibrutinib.

Materials and Methods

Compounds

Idelalisib and ibrutininb were from SelleckChem, and Q-VD-OPh was from Sigma. Details for synthesis of AQX-435 are provided (32). All compounds were dissolved in dimethylsulfoxide (DMSO) for *in vitro* experiments. DMSO was used as a solvent control in all *in vitro* experiments.

CLL samples

Analysis of CLL samples was performed following informed consent and in accordance with Ethics Committee approvals and the Declaration of Helsinki. Heparinized peripheral blood mononuclear cells (PBMC) were obtained from patients attending clinic at the Southampton General Hospital (Supplementary Table 1). All patients provided written informed consent. *IGHV* mutation status, expression of cell surface IgM, CD5, CD19, CD23 and CD38, and ZAP70 were determined as described (9,33). CD49d expression was analyzed by flow cytometry using a FITC-labeled anti-CD49d mouse monoclonal antibody (Biolegend) and calculated as percentage of $CD5^+CD19^+$ cells. sIgM signaling capacity was determined by measuring the percentage of cells with increased intracellular Ca^{2+} (iCa^{2+}) following stimulation with soluble goat $F(ab')_2$ anti-IgM (Southern Biotech) (33).

CLL cells were analyzed using either snap-frozen pellets prepared immediately following isolation of PBMCs (for experiments shown in Fig. 1A and Supplementary Fig. 1) or following recovery of cryopreserved cells (for all other experiments). We previously showed that recovery does not significantly affect anti-IgM responses (9,33,34). PBMCs were also isolated from healthy individuals and cryopreserved before use (34). Cryopreserved PBMCs were recovered and rested for one hour at 37°C prior to use. Cell viability was determined by trypan blue exclusion and was ≥90% in all cases. For BCR stimulation, samples were incubated with soluble or bead-bound goat $F(ab')_2$ anti-human IgM, goat $F(ab')_2$ anti-human IgD or control $F(ab')_2$ (all Southern Biotech) as described (35). CD40L/IL4 stimulation was as described (36).

Cell lines

TMD8 (kind gift of Professor L M Staudt) and WSU-FSCCL and RL (Liebniz Institute DSMZ, Germany) were cultured in RPMI-1640 medium (Sigma) supplemented with 10% (v/v) fetal bovine serum (BioSera) and penicillin, streptomycin and glutamine (all Sigma). Cell line identity was routinely confirmed using short tandem repeat analysis (Powerplex 16 System, Promega) and absence of mycoplasma was confirmed using Mycoplasma PCR

detection kit (Applied Biological Materials). Cell lines were typically cultured for a maximum of 6-8 weeks.

Immunoblotting

SDS-PAGE was performed using equal protein loading following quantitation of protein content using the BioRad Protein Assay. Immunoblot analysis was performed using the following antibodies; anti-ERK1/2, anti–phosphorylated ERK1/2 (T^{202}/Y^{204}), anti-SHIP1, anti-phosphorylated SHIP1 (Y^{1022}), anti-SYK, anti-phosphorylated-SYK ($Y^{525/526}$), anti-AKT, anti-phosphorylated AKT (T^{308} and S^{473}) (all Cell Signaling Technology), anti-MYC (Calbiochem), anti-μ-heavy chain (Jackson ImmunoResearch Laboratories), anti-PARP (BD Biosciences), anti-β-actin (Sigma) and anti-HSC70 (Santa Cruz Biotechnologies). Secondary antibodies were horseradish peroxidase-conjugated anti-rabbit, mouse or goat antibodies (GE Healthcare) and images were captured using the ChemiDoc-It Imaging System with a BioChemi HR camera (UVP). Immunoblot signals were quantified using ImageJ (http://imagej.nih.gov/ij/). Expression of phosphorylated proteins were normalized to the equivalent total protein expression whereas expression of MYC was normalized to β-actin. PARP cleavage was quantified by the proportion of cleaved PARP as a percentage of total PARP expression (ie, cleaved plus uncleaved).

Pull-downs

CLL samples were incubated with bead-bound $F(ab')_2$ anti-IgM or bead-bound control $F(ab')_2$ at 4 °C or 37 °C. Cells were collected by centrifugation and lysed using an NP-40 lysis buffer (0.025 M Tris-HCl, 0.15 M NaCl, 1 mM EDTA, 1% (v/v) NP-40 and 5% (v/v) glycerol with added phosphatase and protease inhibitors (Sigma)). After 1 hour on ice, cells were briefly sonicated and then incubated with RNase-free DNase (Qiagen) for 15 minutes at room temperature. Beads and associated proteins were collected by centrifugation and washed 6 times with cold lysis buffer and boiled in SDS-PAGE sample buffer before analysis using immunoblotting.

In vivo studies

NOD.Cg-*Prkdc*^{scid}*Il2rg*^{tm1Wjl}/SzJ mice (NSG mice) were purchased from The Jackson Laboratory or Charles River Laboratories and maintained in a pathogen-free environment in individually ventilated cages and provided with sterilized food and water. Preliminary toxicity experiments were performed to confirm acceptable tolerability of vehicles/compounds. No adverse effects were observed in these initial assessments (data not shown). For efficacy analysis, adult female NSG mice were inoculated subcutaneously with 10^7 lymphoma cells in phosphate-buffered saline (PBS). Therapy was initiated when all mice developed palpable tumors (termed day 1) and mice were stratified so that treatment arms contained mice with comparable starting calculated tumor volumes. For TMD-based xenografts, AQX-435 was formulated in 4% ethanol, 0.8% 1-methyl-2-pyrrolidinone (Sigma), 12% polyethylene glycol 200 (Sigma) and 83.2% PBS, and administered at 10 mg/kg (intraperitoneal, ip; 0.3 ml per mouse). Animals were dosed in 7-day cycles each comprising 5 days of AQX-435 (10 mg/kg; ip) followed by 2 days with no drug. For PDX-models, AQX-435 was formulated in 15% cremophor EL/10% dimethylacetamide (both Sigma) in saline (which allowed us to increase the administered dose to 50 mg/kg) and was

administered daily (ip; 0.3 ml per mouse). Ibrutinib was formulated in 1% hydroxy-propyl-β-cyclodextrin (Sigma) and administered in all experiment at 25 mg/kg by oral gavage (po; 0.2 ml per mouse). The number of animals per experimental group was 6 for TMD8 xenografts, 8 for VFN-D1 and VFN-D2, and 9 for VFN-D3. Tumor growth was assessed using a digital caliper in three perpendicular dimensions and volume calculated according to the following formula: $\pi/6 \times$ length × width × height. Mouse weights were also recorded. All animals were euthanized when the largest dimension of any tumor exceeded 2 cm. Tumors were then resected and weighed. For immunoblot analysis of AKT phosphorylation in TMD8 tumors, animals (n=3 per arm) were treated with AQX-435 or vehicle on days 1, 2, 4 and 5. Tumors were resected 6 hours following final drug/vehicle administration, disrupted using collagenase/DNase (both Sigma) and lymphoma cells isolated using Lymphoprep (Stemcell Technologies).

Animal experiments were approved by (i) the Institutional Animal Care and Use Committee, the Research and Higher Education section of the Ministry of Education, Youth and Sports of the Czech Republic under MSMT-32441/2018-5 or (ii) by local ethical committees, reporting to the Animal Welfare Ethical Review Board, under UK Home Office license PPL# P4D9C89EA and were fully compliant with the principles of the NC3Rs and the ARRIVE guidelines.

Additional methods are provided in the Supplementary File.

Results

SHIP1 expression and localization in CLL cells

We first characterized SHIP1 expression and Y^{1022} phosphorylation in unstimulated primary CLL cells. Analysis was performed using a cohort of samples comprising both U- and M-CLL, and a range of anti-IgM signal-responsiveness (by analysis of iCa^{2+} mobilization). SHIP1 was expressed and constitutively phosphorylated in all cases (Fig. 1A, Supplementary Fig. 1). Although levels varied between samples, we did not observe statistically significant correlations between SHIP1 expression/phosphorylation and *IGHV* mutation status, signaling capacity or other prognostic markers (CD38, CD49d or ZAP70 expression; Supplementary Fig. 1).

Previous studies have shown that stimulation of the BCR of human or mouse B cells results in rapid phosphorylation of SHIP1, including on Y^{1022} (Y^{1020} in mouse) and relocalization of SHIP1 to the plasma membrane where it is able to access its substrate (2,23,25–27). We therefore investigated the effect of anti-IgM on SHIP1 phosphorylation and subcellular localization using a cohort of samples all of which were considered to be anti-IgM-responsive.

For analysis of SHIP1 phosphorylation, cells were stimulated with soluble or bead-bound anti-IgM. Bead-bound anti-IgM induces stronger and longer-lasting signaling compared to soluble anti-IgM thereby allowing us to probe potential effects of signal strength (35). Both forms of anti-IgM induced AKT phosphorylation and, as expected, the response was stronger in cells treated with bead-bound anti-IgM (Fig. 1B). In most samples, SHIP1 Y^{1022}

phosphorylation was not substantially affected at time points up to 60 minutes post-stimulation (Fig. 1B, Supplementary Fig. 2A,B). However, there was some variation between samples and SHIP1 phosphorylation was increased by ~50% in one sample, and reduced by ~65% in another. Thus, overall, anti-IgM does not consistently promote SHIP1 Y^{1022} phosphorylation in signal-competent CLL samples, although SHIP1 Y^{1022} phosphorylation may be altered (up or down) in a subset of samples. SHIP1 phosphorylation was also essentially unaltered following treatment of two anti-IgM non-responsive samples with soluble or bead-bound anti-IgM (Supplementary Fig. 2C).

Analysis of SHIP1 subcellular localization by microscopy was performed using soluble anti-IgM only since strong autofluorescence of anti-IgM-coated beads precluded the use of this reagent in these experiments. Although phospho-SHIP1 was predominantly localized in the cytoplasm of CLL cells without stimulation (Fig. 1C), anti-IgM triggered re-localization of phospho-SHIP1 to the plasma membrane. Confocal microscopy confirmed the membrane localization of phospho-SHIP1 in anti-IgM-treated cells and additionally demonstrated substantial co-localization of phospho-SHIP1 and sIgM (Fig. 1D).

We performed “pull-down” experiments to determine whether co-localization of phospho-SHIP1 and sIgM was due to association of SHIP1 with activated sIgM complexes. μ-heavy chain precipitations were performed at 4 and 37 °C to investigate both constitutive and activation-induced association (Fig. 1E). Immunoblotting revealed increased binding of both phospho-SYK and phospho-SHIP1 to sIgM in cells at 37 °C whereas μ-heavy chain was precipitated equally under both conditions.

Overall, these results demonstrate that SHIP1 is constitutively expressed and phosphorylated on Y^{1022} in unstimulated CLL cells. sIgM activation does not alter SHIP1 Y^{1022} phosphorylation but leads to recruitment of phospho-SHIP1 to sIgM.

SHIP1 agonist AQX-435 inhibits PI(3,4,5)P_3-mediated signaling following BCR activation

We selected the novel SHIP1 agonist AQX-435 to investigate the effects of SHIP1 activation (Supplementary Fig. 3). AQX-435 is structurally related to pelorol and the closely related compound MN-100, which was synthesized to remove pharmacologically undesirable catechol and ester functionalities (30,37). However, both pelorol and MN-100 have extremely poor water solubility and AQX-435 was produced as part of a panel of new analogues synthesized to improve solubility and other drug-like properties (30,32). AQX-435 was selected from this panel based of its enhanced drug-like properties (including improved aqueous solubility) and the results of initial screens demonstrating effective inhibition of AKT phosphorylation in primary CLL cells (data not shown). We did not use AQX-1125 (which is structurally unrelated to pelorol and was developed as an anti-inflammatory agent) as a tool compound, since it is a relatively weak SHIP1 activator compared to pelorol-related compounds (38,39). Some results have previously been reported in abstract form where AQX-435 was referred to as AQX-C5 (40,41).

We first investigated the effect of AQX-435 on anti-IgM-induced AKT phosphorylation using a set of sIgM signal-responsive CLL samples. We analyzed both AKT T^{308} and S^{473} phosphorylation, although for quantitation we focused on S^{473} due to increased sensitivity of

detection of phosphorylation at this site. Immunoblotting demonstrated that AQX-435 caused a dose-dependent decrease in phosphorylation of AKT at both sites (Fig. 2A). As expected, inhibition of AKT phosphorylation was also observed with idelalisib, although responses were more dramatic that observed with AQX-435 (Fig. 2A, Supplementary Fig. 4). AQX-435 also reduced AKT phosphorylation following ligation of sIgD which is co-expressed with sIgM on CLL cells (Supplementary Fig. 5A,B).

In addition to effects on AKT phosphorylation, AQX-435 significantly reduced anti-IgM-induced phosphorylation of ERK1/2 (Fig. 2B) which is susceptible to inhibition with idelalisib in CLL cells (12), and induction of MYC (Fig. 2C), a downstream target for $PI(3,4,5)P_3$-mediated signaling. By contrast, AQX-435 did not inhibit anti-IgM-induced SYK phosphorylation which is upstream of $PI(3,4,5)P_3$ (Fig. 2D) or anti-IgM-induced iCa^{2+} flux which was also only modestly reduced by idelalisib (Supplementary Fig. 6A,B). AQX-435 also did not alter sIgM expression or increase SHIP1 Y^{1022} phosphorylation (Supplementary Fig. 6C,D).

Therefore, AQX-435 decreases $PI(3,4,5)P_3$-mediated activation of AKT and downstream MYC induction, without substantial effects on upstream SYK phosphorylation or sIgM expression.

AQX-435 and ibrutinib combine effectively to enhanced inhibition of BCR signaling

Combination therapy is an effective strategy to boost responses and we therefore analyzed the effects of combined treatment with AQX-435 and the BTK inhibitor, ibrutinib, on anti-IgM-induced AKT phosphorylation. AQX-435 was tested at 30 μM and ibrutinib was used at 100 nM, a concentration that is readily achieved in the plasma of treated patients and is sufficient to fully occupy the BTK active site and inhibit BTK autophosphorylation in cells *in vitro* (GP, Rachel Arthur, Adam Linley; manuscript submitted). Like AQX-435, ibrutinib only partially inhibited AKT phosphorylation in anti-IgM-treated cells (Fig. 3A,B). However, the combination of AQX-435 and ibrutinib resulted in almost complete inhibition of anti-IgM-induced AKT phosphorylation compared to either agent alone.

We also investigated effects of AQX-435 and/or ibrutinib on the calcium response pathway by analyzing both iCa^{2+} mobilization and phosphorylation of PLCγ2 (which catalyzes production of the iCa^{2+}-liberating second messenger inositol triphosphate). Consistent with previous experiments, AQX-435 had relatively little effect on anti-IgM-induced PLCγ2 phosphorylation and iCa^{2+} release, whereas both responses were very effectively inhibited by ibrutinib (Supplementary Fig. 7A,B). Addition of AQX-435 did not interfere with ibrutinib-mediated inhibition of the calcium response. Therefore, the combination of AQX-435 and ibrutinib results in a more pronounced inhibition of anti-IgM signaling responses compared to either agent alone.

AQX-435 induces caspase-dependent apoptosis and overcomes survival signals

$PI(3,4,5)P_3$-dependent signaling is a key driver of cell survival and we next analyzed the effect of AQX-435 on CLL cell viability using a cohort of 24 CLL samples. AQX-435 reduced CLL cell viability in a dose-dependent manner (Fig. 4A). AQX-435-induced cell killing was somewhat greater in samples from some poor prognosis subsets (U-CLL and

CD38 positive; Supplementary Fig. 8A). AQX-435-induced apoptosis was mediated via caspases since AQX-435 induced PARP cleavage (Fig. 4B,C) and caspase inhibition reduced AQX-435-induced apoptosis (Fig. 4D). In contrast to AQX-435, and consistent with previous findings (42), idelalisib had only very modest pro-apoptotic effects in CLL cells even when tested at concentrations up to 10 μM to ensure full inhibition of AKT phosphorylation (Supplementary Fig. 8B).

CLL cells are exposed to a range of microenvironmental factors *in vivo* which can promote malignant cell survival (43). To determine whether AQX-435 could also induce apoptosis in the presence of these signals, we performed experiments with CD40L and IL4 which promotes CLL cell survival *in vitro* and may mimic potential supportive effects of T cells *in vivo* (36,44,45). Although CD40L/IL4 decreased spontaneous apoptosis of CLL cells, AQX-435 was still able to significantly increase apoptosis in the presence of CD40L/IL4 (Fig. 4E). AQX-435 also overcame the survival promoting effects of bead-bound anti-IgM stimulation (Fig. 4F).

Finally, we investigated effects of AQX-435 on viability of B cells from healthy individuals. Although AQX-435 significantly reduced viability of normal B cells (Fig. 4G), these cells were significantly less sensitive than CLL cells. For example, when comparing DMSO-normalized data (to account for variation in spontaneous apoptosis between normal B cells and CLL cells) the difference in reduction in viability for cells treated with 30 μM AQX-435 was highly statistically significant (P=8.4 x 10^{-6}; Student's t-test; mean ±SD of 17±7% for normal B cells versus 52±25% for CLL cells).

Effect of AQX-435 on BCR signaling in DLBCL cell lines

Having evaluated effects of AQX-435 in CLL, we next investigated whether the inhibitory effects of AQX-435 on BCR signaling extended to other B-cell neoplasms. We focused on DLBCL which is the most common lymphoma subtype and is also frequently characterized by active PI3K signaling (5,13). Moreover, there is a particularly pressing need for new therapeutic options in DLBCL where responses to kinase inhibitors, including idelalisib, are much less dramatic than those observed in CLL.

We selected the ABC-DLBCL cell line TMD8 for initial studies since it depends on BCR signaling for growth (46) and confirmed like that, like idelalisib, AQX-435 inhibited anti-IgM-induced AKT phosphorylation in these cells (Fig. 5A,B). In addition, AQX-435 reduced anti-IgM-induced AKT phosphorylation in a second DLBCL cell line, WSU-FSCCL, derived from a transformed FL (Supplementary Fig. 9).

Next, we screened a panel of DLBCL cell lines, including examples of both GCB and ABC-DLBCL, for AQX-435-induced growth inhibition. Applying a cut-off of 5 μM, 10/11 of the cell lines were considered sensitive to AQX-435-induced growth inhibition (Fig. 5C and Supplementary Table 2). Using annexin V staining, we confirmed that AQX-435 induced TMD8 cell apoptosis *in vitro* with an IC_{50} of ~2 μM (Supplementary Fig. 10A). Thus, in addition to primary CLL cells, AQX-435 reduces anti-IgM-induced AKT phosphorylation and induces apoptosis in DLBCL cells.

In vivo activity of AQX-435 in DLBCL models, alone and in combination with ibrutinib

We analyzed *in vivo* anti-lymphoma effects of AQX-435 using a panel of mice bearing TMD8 or DLBCL PDX tumors. AQX-435 significantly reduced the volume of TMD8 tumors *in vivo* (Fig. 5D, Supplementary Table 7) and tumor weight at the end of the experiment (Fig. 5E). Efficacy of AQX-435 was very similar to ibrutinib. There was no evidence for toxicity in terms of reduced body weight (Supplementary Fig. 10B) or gross signs of toxicity with either agent. We also examined the levels of AKT phosphorylation in lymphoma cells from animals treated with AQX-435 or vehicle (n=3 for each; Fig. 5F, Supplementary Fig. 10C). We were unable to obtain intact protein from one tumor from the AQX-435-treated mice. However, AKT phosphorylation in the remaining two tumors was substantially reduced (~50%) compared to controls.

Next, three different PDX models derived from patients with treatment-refractory DLBCL (VFN-D1, VFN-D2) or DLBCL at diagnosis (VFN-D3) were used to assess anti-tumor activity of AQX-435. Experiments were performed using AQX-435 as a single-agent, but also in combination with ibrutinib since previous studies have shown increased efficacy of ibrutinib with PI3Ki (47). Detailed molecular characterization of the PDX models is given in Supplementary Tables 3-6 and Supplementary Fig. 11.

Consistent with the differing cell-or-origin and genetic make-up, response to AQX-435 and/or ibrutinib differed between the models. AQX-435 had substantial inhibitory effects on tumor growth in VFN-D2 and VFN-D3 but was less effective in VFN-D1 (Fig. 6A-C, Supplementary Table 7). Ibrutinib was essentially inactive in VFN-D2 (GCB subtype) and had similar activity to AQX-435 in the other two models (both non-GCB subtype). Importantly, the combination of AQX-435 and ibrutinib further reduced tumor volume in the non-GCB PDX models VFN-D1 and VFN-D3 (but not in GCB PDX model VFN-D2 where ibrutinib was essentially inactive as a monotherapy). Enhanced activity of the AQX-435/ibrutinib combination was particularly striking in the VFN-D1 model, resulting in profound and durable (>14 days) tumor regression. Effects of AQX-435 (±ibrutinib) on tumor volume were accompanied by significant reductions in tumor weight at the end of the experiments in all three models (Fig. 6D) and there was no evidence for toxicity in terms of reduced body weight (Supplementary Fig. 12). Thus, AQX-435 has promising activity against DLBCL and can be combined effectively with ibrutinib to enhance anti-tumor activity.

Discussion

In this study, we explored the novel strategy of phosphatase activation to inhibit BCR signaling using the SHIP1 activator AQX-435. Previous studies using the SHIP1 agonist MN-100 have demonstrated induction of apoptosis in multiple myeloma cell lines *in vitro* (29,31). However, the effects of pharmacological SHIP1 activation on BCR signaling and *in vivo* anti-tumor activity of SHIP1 agonists have not been reported. We show for the first time that SHIP1 activation using AQX-435 effectively inhibits PI(3,4,5)P_3-mediated signaling downstream of the BCR in CLL and DLBCL cells. Moreover, AQX-435 promotes apoptosis of primary CLL cells with relative specificity compared to normal counterparts, and is well tolerated and efficacious in *in vivo* models of DLBCL, including in combination with ibrutinib. Thus, SHIP1 activation is a potential new therapeutic approach to inhibit

inappropriate PI3K-mediated signaling, with activity across several distinct subtypes of B-cell neoplasms.

AQX-435 was selected from a panel of new synthetic pelorol analogues synthesized to generate new SHIP1 agonists with improved water solubility and other drug-like properties compared to previous agents, including pelorol itself and MN-100 (30,32,37). In particular, AQX-435 has much improved water solubility compared to previous pelorol-related SHIP1 agonists and retains good ability to suppress PI(3,4,5)P_3-mediated signaling in intact cells. Moreover, it can be formulated for *in vivo* administration to achieve doses that are sufficient to limit lymphoma growth without substantial toxicity.

Profiling of primary samples demonstrated that SHIP1 was widely expressed and phosphorylated in CLL cells. Levels were variable but were not clearly different between disease subtypes. We were unable to confirm results of a previous study demonstrating that SHIP1 expression/phosphorylation was higher in ZAP70 positive versus negative cases (48). However, quantitative analysis in that study was based on only a small number of samples. Moreover, although *miR-155* suppresses SHIP1 expression and is expressed more highly in U-CLL (49), we also did not observe a correlation between SHIP1 expression and *IGHV* mutation status. Although we cannot exclude the possibility that larger studies may reveal some quantitative differences in SHIP1 expression/phosphorylation between disease subtypes, constitutive SHIP1 expression/phosphorylation largely appears to be a general feature of CLL cells.

Plasma membrane localization is critical for SHIP1 function since it is required for substrate access and, in normal B cells, BCR stimulation induces rapid phosphorylation of SHIP1, including on Y^{1022}, and relocalization to the plasma membrane (2,23,25–27). Anti-IgM stimulation of CLL cells also triggered plasma membrane re-localization of SHIP1 and association with activated BCRs. However, it was interesting to note that SHIP1 was constitutively phosphorylated on Y^{1022} in CLL cells and that phosphorylation was not further increased by stimulation *in vitro*. It is possible that this constitutive phosphorylation of SHIP1 is due to (auto)antigen engagement of CLL cell BCRs *in vivo*, or engagement of other receptors which can induce Y^{1022} phosphorylation, such as FcγRIIB (2). Constitutive Y^{1022} phosphorylation may therefore prime CLL cells for full activation following BCR activation but membrane recruitment may require additional steps. One possibility is that activation of the BCR triggers recruitment of pre-existing phospho-SHIP1 via binding of the SHIP1 SH2 domains to tyrosine phosphorylated residues in the ITAM motifs of CD79A/B (the signal transduction components of the BCR) (2,27).

Consistent with shared ability to reduce concentrations of PI(3,4,5)P_3, AQX-435 and idelalisib exerted similar effects on BCR signaling in primary CLL cells (ie, inhibition of AKT and ERK phosphorylation without effects on upstream SYK phosphorylation or parallel iCa^{2+} mobilization). However, higher concentrations were required for AQX-435 action compared to idelalisib. Differences in potency/efficacy of AQX-435 and idelalisib are likely to be multifactorial, but may reflect, at least in part, the differing modes of action of these agents. Thus, increasing idelalisib concentrations will ultimately lead to full PI3K blockade once all of the kinase active sites have been occupied. By contrast, the inhibitory

effects of AQX-435 are limited by the availability of SHIP1; once the available SHIP1 is fully activated addition of further compound will not enhance inhibitory effects. It is also important to consider that, in contrast to PI3Ki, SHIP1 does not block production of $PI(3,4,5)P_3$, but accelerates its breakdown. Thus, even when SHIP1 is fully activated, there remains a transient "window" in which $PI(3,4,5)P_3$ may engage downstream effectors prior to its breakdown. However, although relatively high AQX-435 concentrations were required to inhibit signaling in CLL cells, low μM concentrations were sufficient for growth inhibitory effects in most lymphoma cell lines analyzed and for induction of apoptosis of TMD8 cells and our analysis clearly demonstrated that it was possible to achieve concentrations sufficient to reduce AKT phosphorylation and tumor growth *in vivo* with no evidence for substantial toxicity. Notably, AQX-435 had broad activity against a panel of DLBCL cell lines; the ability of SHIP1 activation to counter $PI(3,4,5)P_3$-mediated signaling regardless of the specific PI3K isoform(s) that mediate $PI(3,4,5)P_3$ synthesis may account for this activity, whereas inhibition of multiple PI3K isoforms is generally required for effective growth inhibition (17).

Consistent with a key role for $PI(3,4,5)P_3$-mediated signaling in cell survival, AQX-435 induced caspase-dependent apoptosis of CLL cells and overcame survival promoting effects of both anti-IgM and CD40L/IL4. Interestingly, CLL cells were significantly more susceptible to AQX-435-induced apoptosis than non-malignant B cells. Future experiments will explore whether the enhanced sensitivity of CLL cells may be linked to constitutive Y^{1022} phosphorylation. AQX-435 also appeared to have stronger pro-apoptotic effects than idelalisib which only very modestly induced cell killing even at relatively high concentrations. The increased pro-apoptotic activity of AQX-435 compared to idelalisib could be mediated by combined depletion of $PI(3,4,5)P_3$ and accumulation of $PI(3,4)P_2$.

We extended our analysis to DLBCL, including for *in vivo* assessment. It was important to assess activity of AQX-435 in this setting, since, in contrast to CLL, targeted agents (including idelalisib) are relatively ineffective as a monotherapies in DLBCL, and effective combinations are important to boost therapeutic responses. We demonstrated that AQX-435 alone reduced lymphoma growth *in vivo* using the TMD8 cell line and three new DLBCL PDX models. Enhanced activity of the combination of AQX-435 and ibrutinib was observed in 2 of the 3 PDX models and was particularly striking in VFN-D1 which showed clear evidence for tumor regression with the combination. The mechanism underlying the enhanced efficacy of the combination of AQX-435 and ibrutinib is unclear but may stem from the more pronounced inhibition of AKT phosphorylation by the combination compared to either agent alone, as observed in CLL cells. Variable drug responsiveness between the PDX models may stem from differences in cell-of-origin (ie, GCB versus non-GCB) and it was notable that growth of VFN-D2 tumors, derived from GCB-DLBCL, appeared to be unaffected by ibrutinib since patients with GCB-DLBCL are less responsive to ibrutinib therapy compared to ABC-DLBCL (50).

Overall, our results demonstrate that SHIP1 activation is a potential new therapeutic approach for B-cell neoplasms characterized by PI3K activation, alone or in combination with ibrutinib. It has broad growth inhibitory activity against DLBCL, which may reflect its ability (unlike idelalisib) to reduce $PI(3,4,5)P_3$-mediated signaling independent of the

particular PI3K isoform(s) that catalyze PI(3,4,5)P_3 accumulation. It also has stronger pro-apoptotic activity which may relate to its ability to drive accumulation of PI(3,4)P_2. Further experiments, particularly using immunocompetent animals, will be required to determine whether the differing modes of action of idelalisib and AQX-435 (which appears to cause a more nuanced attenuation of PI(3,4,5)P_3-mediated signaling) translate into reduced toxicity, and the relative effectiveness of AQX-435 versus PI3Ki in combination with ibrutinib.

Supplementary Material

Refer to Web version on PubMed Central for supplementary material.

Acknowledgements

We thank the patients involved in this study for the kind gift of samples and Dr Ian Tracy, Mrs Isla Henderson, Dr Kathy Potter and Ms Carina Mundy for characterization and storage of the CLL samples, and Dr Patrick Duriez for providing annexin V. We thanks Professor L Staudt for the kind gift of TMD8 cells. This work was supported by grants from Cancer Research UK (C2750/A23669), Bloodwise (14045, 16004, 16003, 18009), Kay Kendall Leukaemia Fund (KKL0168), Aquinox Pharmaceuticals (Canada) Inc., the Southampton Experimental Cancer Medicine and Cancer Research Centres (C24563/A15581; C34999/A18087), UNCE/MED/016, GACR17-14007S and the Keanu Eyles Haematology Fellowship for the Cancer Immunology Centre.

Financial support. This work was supported by grants from Cancer Research UK (C2750/A23669), Bloodwise (14045, 16004, 16003, 18009), Kay Kendall Leukaemia Fund (KKL0168), Aquinox Pharmaceuticals (Canada) Inc., the Southampton Experimental Cancer Medicine and Cancer Research Centres (C24563/A15581; C34999/A18087), UNCE/MED/016, GACR17-14007S and the Keanu Eyles Haematology Fellowship for the Cancer Immunology Centre.

References

1. Okkenhaug K. Signaling by the phosphoinositide 3-kinase family in immune cells. Annu Rev Immunol. 2013; 31:675–704. DOI: 10.1146/annurev-immunol-032712-095946 [PubMed: 23330955]
2. Pauls SD, Marshall AJ. Regulation of immune cell signaling by SHIP1: A phosphatase, scaffold protein, and potential therapeutic target. Eur J Immunol. 2017; 47(6):932–45. DOI: 10.1002/eji.201646795 [PubMed: 28480512]
3. Landego I, Jayachandran N, Wullschleger S, Zhang TT, Gibson IW, Miller A, et al. Interaction of TAPP adapter proteins with phosphatidylinositol (3,4)-bisphosphate regulates B-cell activation and autoantibody production. Eur J Immunol. 2012; 42(10):2760–70. DOI: 10.1002/eji.201242371 [PubMed: 22777911]
4. Jerkeman M, Hallek M, Dreyling M, Thieblemont C, Kimby E, Staudt L. Targeting of B-cell receptor signalling in B-cell malignancies. J Intern Med. 2017; 282(5):415–28. DOI: 10.1111/joim.12600 [PubMed: 28295729]
5. Havranek O, Xu J, Kohrer S, Wang Z, Becker L, Comer JM, et al. Tonic B-cell receptor signaling in diffuse large B-cell lymphoma. Blood. 2017; 130(8):995–1006. DOI: 10.1182/blood-2016-10-747303 [PubMed: 28646116]
6. Petlickovski A, Laurenti L, Li XP, Marietti S, Chiusolo P, Sica S, et al. Sustained signaling through the B-cell receptor induces Mcl-1 and promotes survival of chronic lymphocytic leukemia B cells. Blood. 2005; 105(12):4820–7. DOI: 10.1182/blood-2004-07-2669 [PubMed: 15728130]
7. Linley A, Krysov S, Ponzoni M, Johnson PW, Packham G, Stevenson FK. Lectin binding to surface Ig variable regions provides a universal persistent activating signal for follicular lymphoma cells. Blood. 2015; 126(16):1902–10. DOI: 10.1182/blood-2015-04-640805 [PubMed: 26194765]
8. Amin R, Mourcin F, Uhel F, Pangault C, Ruminy P, Dupre L, et al. DC-SIGN-expressing macrophages trigger activation of mannosylated IgM B-cell receptor in follicular lymphoma. Blood. 2015; 126(16):1911–20. DOI: 10.1182/blood-2015-04-640912 [PubMed: 26272216]

Europe PMC Funders Author Manuscripts

9. Lanham S, Hamblin T, Oscier D, Ibbotson R, Stevenson F, Packham G. Differential signaling via surface IgM is associated with VH gene mutational status and CD38 expression in chronic lymphocytic leukemia. Blood. 2003; 101(3):1087–93. DOI: 10.1182/blood-2002-06-1822 [PubMed: 12393552]
10. D'Avola A, Drennan S, Tracy I, Henderson I, Chiecchio L, Larrayoz M, et al. Surface IgM expression and function are associated with clinical behavior, genetic abnormalities, and DNA methylation in CLL. Blood. 2016; 128(6):816–26. DOI: 10.1182/blood-2016-03-707786 [PubMed: 27301861]
11. Herman SE, Gordon AL, Hertlein E, Ramanunni A, Zhang X, Jaglowski S, et al. Bruton tyrosine kinase represents a promising therapeutic target for treatment of chronic lymphocytic leukemia and is effectively targeted by PCI-32765. Blood. 2011; 117(23):6287–96. DOI: 10.1182/blood-2011-01-328484 [PubMed: 21422473]
12. Hoellenriegel J, Meadows SA, Sivina M, Wierda WG, Kantarjian H, Keating MJ, et al. The phosphoinositide 3'-kinase delta inhibitor, CAL-101, inhibits B-cell receptor signaling and chemokine networks in chronic lymphocytic leukemia. Blood. 2011; 118(13):3603–12. DOI: 10.1182/blood-2011-05-352492 [PubMed: 21803855]
13. Pfeifer M, Grau M, Lenze D, Wenzel SS, Wolf A, Wollert-Wulf B, et al. PTEN loss defines a PI3K/AKT pathway-dependent germinal center subtype of diffuse large B-cell lymphoma. Proc Natl Acad Sci U S A. 2013; 110(30):12420–5. DOI: 10.1073/pnas.1305656110 [PubMed: 23840064]
14. Zirlik K, Veelken H. Idelalisib. Recent Results Cancer Res. 2018; 212:243–64. DOI: 10.1007/978-3-319-91439-8_12 [PubMed: 30069634]
15. Greenwell IB, Ip A, Cohen JB. PI3K Inhibitors: Understanding Toxicity Mechanisms and Management. Oncology (Williston Park). 2017; 31(11):821–8. [PubMed: 29179250]
16. de Weerdt I, Koopmans SM, Kater AP, van Gelder M. Incidence and management of toxicity associated with ibrutinib and idelalisib: a practical approach. Haematologica. 2017; 102(10):1629–39. DOI: 10.3324/haematol.2017.164103 [PubMed: 28775119]
17. Erdmann T, Klener P, Lynch JT, Grau M, Vockova P, Molinsky J, et al. Sensitivity to PI3K and AKT inhibitors is mediated by divergent molecular mechanisms in subtypes of DLBCL. Blood. 2017; 130(3):310–22. DOI: 10.1182/blood-2016-12-758599 [PubMed: 28202458]
18. Krause G, Hassenruck F, Hallek M. Copanlisib for treatment of B-cell malignancies: the development of a PI3K inhibitor with considerable differences to idelalisib. Drug Des Devel Ther. 2018; 12:2577–90. DOI: 10.2147/DDDT.S142406
19. Flinn IW, O'Brien S, Kahl B, Patel M, Oki Y, Foss FF, et al. Duvelisib, a novel oral dual inhibitor of PI3K-delta,gamma, is clinically active in advanced hematologic malignancies. Blood. 2018; 131(8):877–87. DOI: 10.1182/blood-2017-05-786566 [PubMed: 29191916]
20. Yahiaoui A, Meadows SA, Sorensen RA, Cui ZH, Keegan KS, Brockett R, et al. PI3Kdelta inhibitor idelalisib in combination with BTK inhibitor ONO/GS-4059 in diffuse large B cell lymphoma with acquired resistance to PI3Kdelta and BTK inhibitors. PLoS One. 2017; 12(2):e0171221.doi: 10.1371/journal.pone.0171221 [PubMed: 28178345]
21. de Rooij MF, Kuil A, Kater AP, Kersten MJ, Pals ST, Spaargaren M. Ibrutinib and idelalisib synergistically target BCR-controlled adhesion in MCL and CLL: a rationale for combination therapy. Blood. 2015; 125(14):2306–9. DOI: 10.1182/blood-2014-12-619163 [PubMed: 25838279]
22. Liu Q, Oliveira-Dos-Santos AJ, Mariathasan S, Bouchard D, Jones J, Sarao R, et al. The inositol polyphosphate 5-phosphatase ship is a crucial negative regulator of B cell antigen receptor signaling. J Exp Med. 1998; 188(7):1333–42. DOI: 10.1084/jem.188.7.1333 [PubMed: 9763612]
23. Brauweiler A, Tamir I, Dal Porto J, Benschop RJ, Helgason CD, Humphries RK, et al. Differential regulation of B cell development, activation, and death by the src homology 2 domain-containing 5' inositol phosphatase (SHIP). J Exp Med. 2000; 191(9):1545–54. DOI: 10.1084/jem.191.9.1545 [PubMed: 10790429]
24. O'Neill SK, Getahun A, Gauld SB, Merrell KT, Tamir I, Smith MJ, et al. Monophosphorylation of CD79a and CD79b ITAM motifs initiates a SHIP-1 phosphatase-mediated inhibitory signaling cascade required for B cell anergy. Immunity. 2011; 35(5):746–56. DOI: 10.1016/j.immuni.2011.10.011 [PubMed: 22078222]

25. Manno B, Oellerich T, Schnyder T, Corso J, Losing M, Neumann K, et al. The Dok-3/Grb2 adaptor module promotes inducible association of the lipid phosphatase SHIP with the BCR in a coreceptor-independent manner. Eur J Immunol. 2016; 46(11):2520–30. DOI: 10.1002/eji.201646431 [PubMed: 27550373]
26. Khalil AM, Cambier JC, Shlomchik MJ. B cell receptor signal transduction in the GC is short-circuited by high phosphatase activity. Science. 2012; 336(6085):1178–81. DOI: 10.1126/science.1213368 [PubMed: 22555432]
27. Pauls SD, Ray A, Hou S, Vaughan AT, Cragg MS, Marshall AJ. FcgammaRIIB-Independent Mechanisms Controlling Membrane Localization of the Inhibitory Phosphatase SHIP in Human B Cells. J Immunol. 2016; 197(5):1587–96. DOI: 10.4049/jimmunol.1600105 [PubMed: 27456487]
28. Viernes DR, Choi LB, Kerr WG, Chisholm JD. Discovery and development of small molecule SHIP phosphatase modulators. Med Res Rev. 2014; 34(4):795–824. DOI: 10.1002/med.21305 [PubMed: 24302498]
29. Kennah M, Yau TY, Nodwell M, Krystal G, Andersen RJ, Ong CJ, et al. Activation of SHIP via a small molecule agonist kills multiple myeloma cells. Exp Hematol. 2009; 37(11):1274–83. DOI: 10.1016/j.exphem.2009.08.001 [PubMed: 19703514]
30. Meimetis LG, Nodwell M, Yang L, Wang XX, Wu J, Harwig C, et al. Synthesis of SHIP1-Activating Analogs of the Sponge Meroterpenoid Pelorol. European Journal of Organic Chemistry. 2012; 2012(27):5195–207. DOI: 10.1002/ejoc.201200631
31. Ong CJ, Ming-Lum A, Nodwell M, Ghanipour A, Yang L, Williams DE, et al. Small-molecule agonists of SHIP1 inhibit the phosphoinositide 3-kinase pathway in hematopoietic cells. Blood. 2007; 110(6):1942–9. DOI: 10.1182/blood-2007-03-079699 [PubMed: 17502453]
32. Mackenzie LF, MacRury T, Harwig C, Bogucki D, Raymond J, Pettigrew JD, et al. SHIP1 MODULATORS AND METHODS RELATED THERETO. 2014
33. Mockridge CI, Potter KN, Wheatley I, Neville LA, Packham G, Stevenson FK. Reversible anergy of sIgM-mediated signaling in the two subsets of CLL defined by VH-gene mutational status. Blood. 2007; 109(10):4424–31. DOI: 10.1182/blood-2006-11-056648 [PubMed: 17255355]
34. Yeomans A, Thirdborough SM, Valle-Argos B, Linley A, Krysov S, Hidalgo MS, et al. Engagement of the B-cell receptor of chronic lymphocytic leukemia cells drives global and MYC-specific mRNA translation. Blood. 2016; 127(4):449–57. DOI: 10.1182/blood-2015-07-660969 [PubMed: 26491071]
35. Krysov S, Steele AJ, Coelho V, Linley A, Sanchez Hidalgo M, Carter M, et al. Stimulation of surface IgM of chronic lymphocytic leukemia cells induces an unfolded protein response dependent on BTK and SYK. Blood. 2014; 124(20):3101–9. DOI: 10.1182/blood-2014-04-567198 [PubMed: 25170122]
36. Blunt MD, Koehrer S, Dobson RC, Larrayoz M, Wilmore S, Hayman A, et al. The Dual Syk/JAK Inhibitor Cerdulatinib Antagonizes B-cell Receptor and Microenvironmental Signaling in Chronic Lymphocytic Leukemia. Clin Cancer Res. 2017; 23(9):2313–24. DOI: 10.1158/1078-0432.CCR-16-1662 [PubMed: 27697994]
37. Yang L, Williams DE, Mui A, Ong C, Krystal G, van Soest R, et al. Synthesis of pelorol and analogues: activators of the inositol 5-phosphatase SHIP. Org Lett. 2005; 7(6):1073–6. DOI: 10.1021/ol047316m [PubMed: 15760142]
38. Stenton GR, Mackenzie LF, Tam P, Cross JL, Harwig C, Raymond J, et al. Characterization of AQX-1125, a small-molecule SHIP1 activator: Part 2. Efficacy studies in allergic and pulmonary inflammation models in vivo. Br J Pharmacol. 2013; 168(6):1519–29. DOI: 10.1111/bph.12038 [PubMed: 23121409]
39. Stenton GR, Mackenzie LF, Tam P, Cross JL, Harwig C, Raymond J, et al. Characterization of AQX-1125, a small-molecule SHIP1 activator: Part 1. Effects on inflammatory cell activation and chemotaxis in vitro and pharmacokinetic characterization in vivo. Br J Pharmacol. 2013; 168(6):1506–18. DOI: 10.1111/bph.12039 [PubMed: 23121445]
40. Packham G, Lemm E, Valle-Argos B, Smith L, Weston-Bell N, Stevenson F, et al. Development of pelorol analogues to activate the SHIP1 lipid phosphatase; a novel paradigm to suppress B-cell receptor signaling in human B-cell cancers. Cancer Research. 2018; 78(13)doi: 10.1158/1538-7445.Am2018-1871

41. Packham G, Valle-Argos B, Lemm E, Smith LD, Weston-Bell NJ, Gebreselassie Y, et al. Chemical Activation of the SHIP1 Inositol Lipid Phosphatase: A Novel Therapeutic Strategy to Suppress B-Cell Receptor Signaling and CXCR4 Expression in Malignant Human B Cells. Blood. 2016; 128(22):2037.

42. Herman SE, Gordon AL, Wagner AJ, Heerema NA, Zhao W, Flynn JM, et al. Phosphatidylinositol 3-kinase-delta inhibitor CAL-101 shows promising preclinical activity in chronic lymphocytic leukemia by antagonizing intrinsic and extrinsic cellular survival signals. Blood. 2010; 116(12):2078–88. DOI: 10.1182/blood-2010-02-271171 [PubMed: 20522708]

43. Burger JA, Gribben JG. The microenvironment in chronic lymphocytic leukemia (CLL) and other B cell malignancies: insight into disease biology and new targeted therapies. Semin Cancer Biol. 2014; 24:71–81. DOI: 10.1016/j.semcancer.2013.08.011 [PubMed: 24018164]

44. Ghia P, Chiorazzi N, Stamatopoulos K. Microenvironmental influences in chronic lymphocytic leukaemia: the role of antigen stimulation. J Intern Med. 2008; 264(6):549–62. DOI: 10.1111/j.1365-2796.2008.02030.x [PubMed: 19017179]

45. Os A, Burgler S, Ribes AP, Funderud A, Wang D, Thompson KM, et al. Chronic lymphocytic leukemia cells are activated and proliferate in response to specific T helper cells. Cell Rep. 2013; 4(3):566–77. DOI: 10.1016/j.celrep.2013.07.011 [PubMed: 23933259]

46. Young RM, Wu T, Schmitz R, Dawood M, Xiao W, Phelan JD, et al. Survival of human lymphoma cells requires B-cell receptor engagement by self-antigens. Proc Natl Acad Sci U S A. 2015; 112(44):13447–54. DOI: 10.1073/pnas.1514944112 [PubMed: 26483459]

47. Niemann CU, Mora-Jensen HI, Dadashian EL, Krantz F, Covey T, Chen SS, et al. Combined BTK and PI3Kdelta Inhibition with Acalabrutinib and ACP-319 Improves Survival and Tumor Control in CLL Mouse Model. Clin Cancer Res. 2017; 23(19):5814–23. DOI: 10.1158/1078-0432.CCR-17-0650 [PubMed: 28645939]

48. Gabelloni ML, Borge M, Galletti J, Canones C, Fernandez Calotti P, Bezares RF, et al. SHIP-1 protein level and phosphorylation status differs between CLL cells segregated by ZAP-70 expression. Br J Haematol. 2008; 140(1):117–9. DOI: 10.1111/j.1365-2141.2007.06891.x [PubMed: 18005265]

49. Cui B, Chen L, Zhang S, Mraz M, Fecteau JF, Yu J, et al. MicroRNA-155 influences B-cell receptor signaling and associates with aggressive disease in chronic lymphocytic leukemia. Blood. 2014; 124(4):546–54. DOI: 10.1182/blood-2014-03-559690 [PubMed: 24914134]

50. Wilson WH, Young RM, Schmitz R, Yang Y, Pittaluga S, Wright G, et al. Targeting B cell receptor signaling with ibrutinib in diffuse large B cell lymphoma. Nat Med. 2015; 21(8):922–6. DOI: 10.1038/nm.3884 [PubMed: 26193343]

Europe PMC Funders Author Manuscripts

Translational relevance

Phosphatidylinositol-3 kinase (PI3K) signaling is activated in various subtypes of B-cell neoplasms where it is an important driver of proliferation and survival of malignant cells. PI3K inhibitors have been introduced into clinical practice, however, there remains a clear need for new drug strategies to target PI3K signaling. For example, treatment with the PI3Kδ-specific inhibitor idelalisib can be associated with substantial toxicity and idelalisib is relatively ineffective as a monotherapy in diffuse large B cell lymphoma (DLBCL). PI3K activity is naturally countered by the inositol lipid phosphatase SHIP1 and, in this study, we show that the novel chemical SHIP1 activator AQX-435 effectively inhibited PI3K signaling in both primary chronic lymphocytic cells and DLBCL-derived cell lines, and reduced growth of lymphoma *in vivo*, alone and in combination with the BTK inhibitor ibrutinib. Thus, SHIP1 activation may present a novel paradigm to inhibit PI3K signaling in B-cell neoplasms.

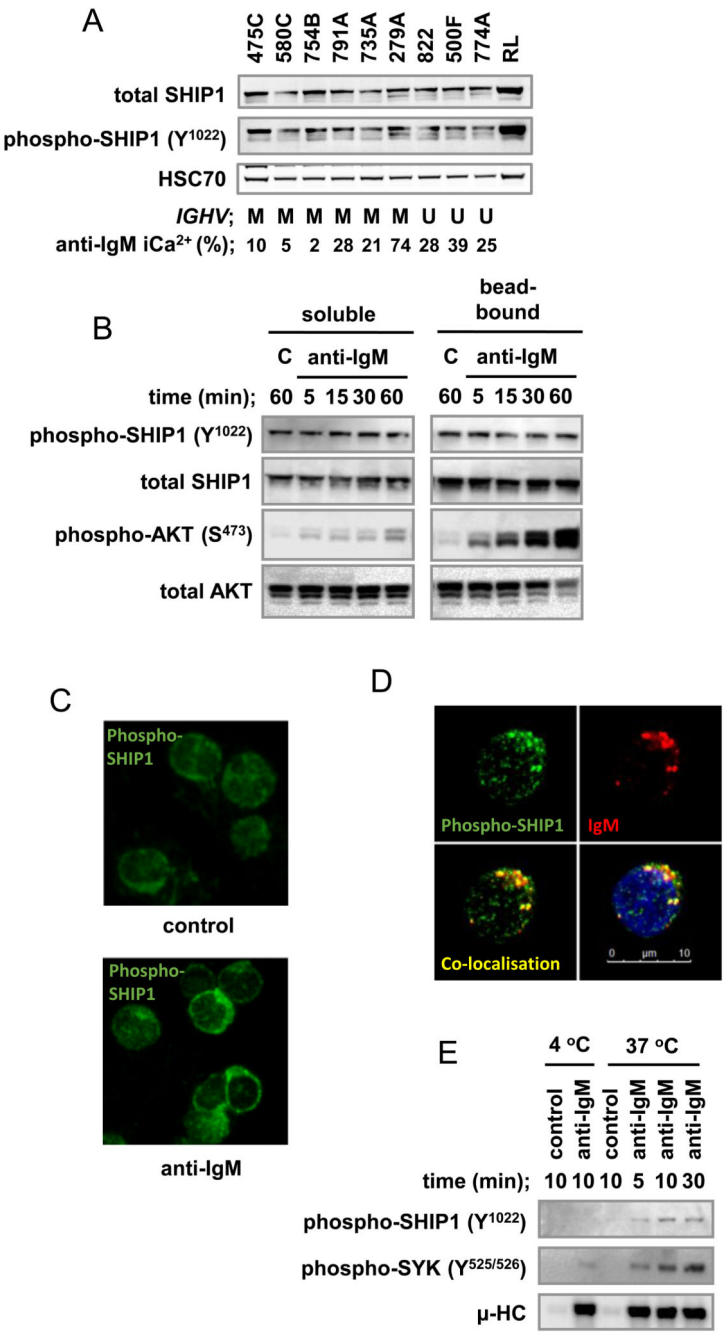

Figure 1.

Characterization of SHIP1 in primary CLL samples. **A,** Lysates were prepared from CLL samples or RL cells (positive control), and expression of total and phospho-SHIP1, and HSC70 (loading control) was analyzed using immunoblotting. Figure shows results for 9 representative samples from a total of 41 (total SHIP1) or 29 (phospho-SHIP1) samples analyzed with *IGHV* mutation status (M, mutated; U, unmutated) and anti-IgM signaling capacity (iCa^{2+}, percent responding cells; Ref. (33) indicated. **B,** CLL samples were treated with soluble or bead-bound anti-IgM or control (C) antibodies for the indicated times.

Expression of total and phospho-SHIP1 and total and phospho-AKT (S^{473}) was analyzed by immunoblotting. Fig. shows results for 1 representative sample from a total of 8 samples analyzed. **C** and **D,** CLL samples were treated with soluble anti-IgM at 37 °C for 30 minutes, or left untreated as a control. Fixed cells were stained with anti-phospho-SHIP1 and then secondary antibodies to detect bound anti-phospho-SHIP1 or anti-IgM. **C,** Phospho-SHIP1 expression (±anti-IgM) in a representative sample of 7 samples analyzed. **D,** Confocal microscopy of anti-IgM-treated cells; anti-phospho-SHIP1 (green), anti-IgM (red) and/or DAPI stained (blue) anti-IgM-treated cells. In merged images (bottom row), co-localization of anti-phospho-SHIP1 and anti-IgM staining is shown in yellow, with or without DAPI staining. Image shown is representative of 5 samples analyzed. **E,** CLL samples were incubated with bead-bound anti-IgM or control antibody at 4 °C or 37 °C for the indicated times. Beads were collected by centrifugation and bound heavy-chain (μ-HC), phospho-SHIP1 and phospho-SYK were analyzed by immunoblotting. Results shown are representative of 2 samples analyzed.

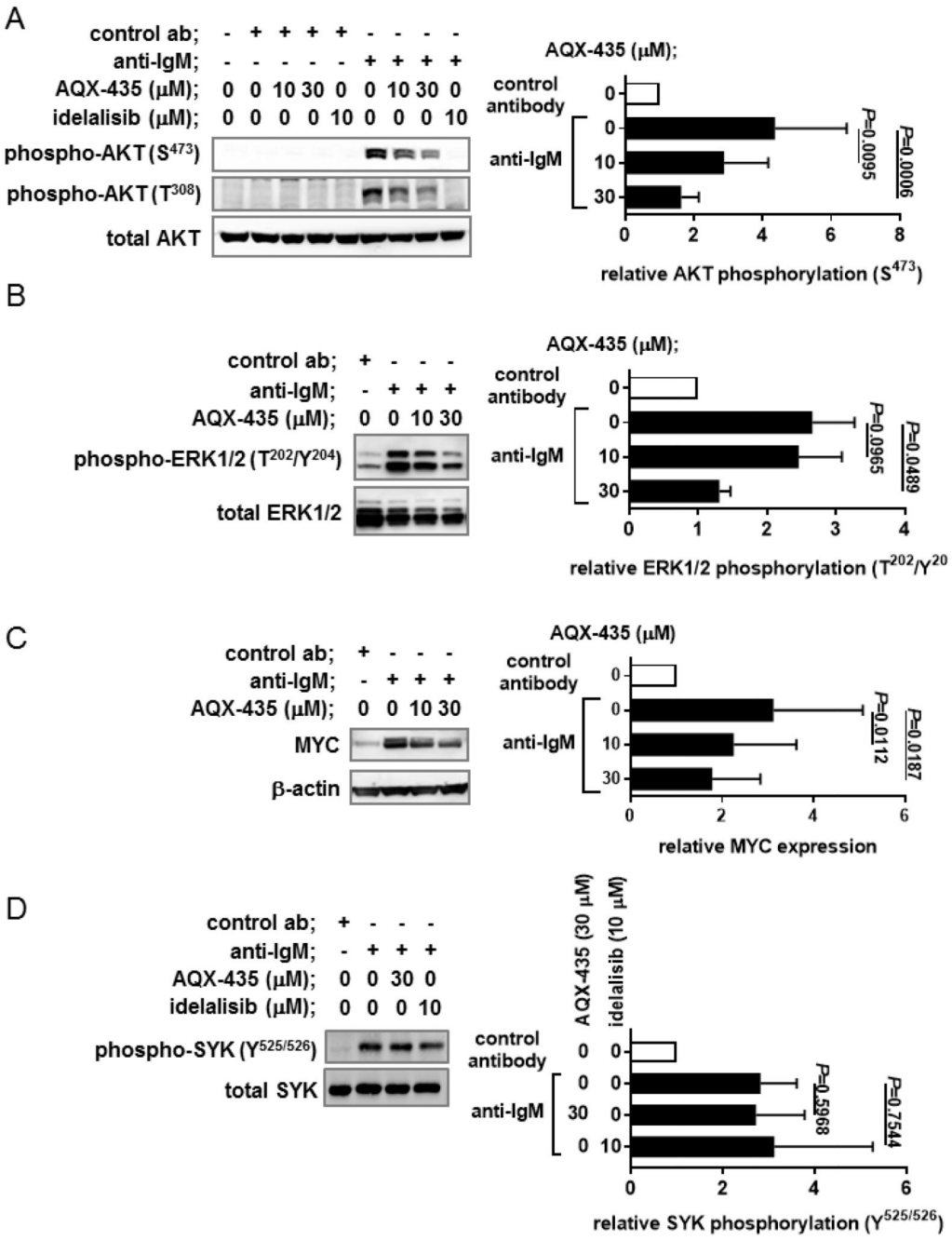

Figure 2.

Effects of AQX-435 on anti-IgM-induced signaling. CLL samples were pre-treated with the indicated concentrations of AQX-435 or idelalisib, or DMSO as a control, for 30 minutes and then stimulated with bead-bound anti-IgM or control antibody (ab). Figures show representative immunoblot analysis and quantitation for all samples analyzed for **A,** total/phospho-AKT (n=11) at 30 minutes after stimulation, **B,** total/phospho-ERK1/2 (n=9) and **C,** MYC (n=9) at 3 hours after stimulation, and **D,** total/phospho-SYK (n=3) at 2 minutes after stimulation. Graphs show mean (±SD) phosphorylation/expression with values for

control antibody/DMSO-treated cells set to 1.0, and the statistical significance of the indicated differences (Student’s t-test).

Europe PMC Funders Author Manuscripts

Europe PMC Funders Author Manuscripts

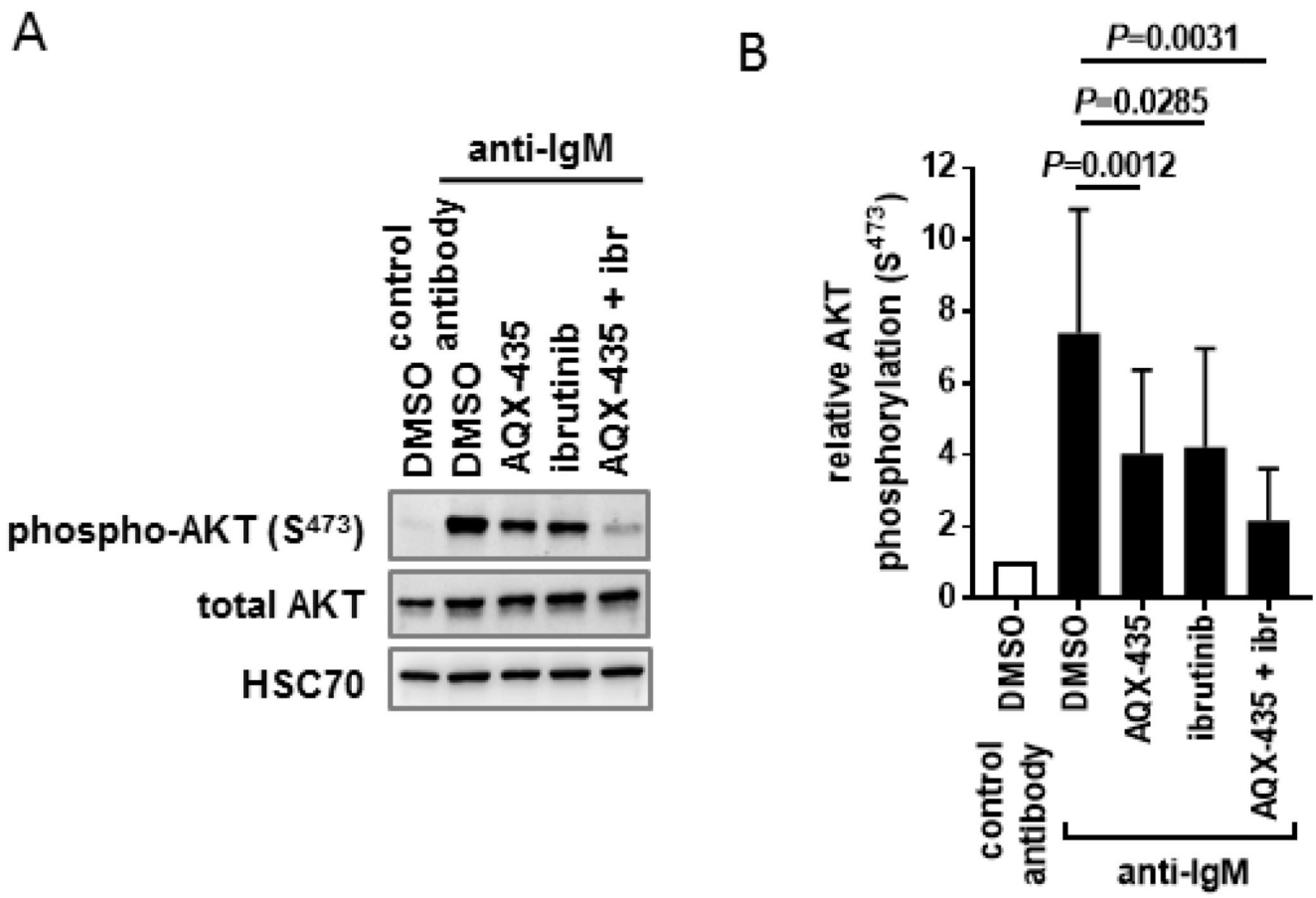

Figure 3.

Effect of combined treatment with AQX-435 and ibrutinib on anti-IgM-induced AKT phosphorylation. **A** and **B,** CLL samples were pre-treated with AQX-435 (30 μM) and/or ibrutinib (100 nM), or DMSO as a control, for 30 minutes. Cells were then stimulated with bead-bound anti-IgM or control antibody for 15 minutes and expression of total/ phospho-AKT (S^{473}) was analyzed by immunoblotting. HSC70 was also analyzed as an additional loading control. **A,** Representative results and **B,** quantitation for all samples analyzed (n=8). Graph shows mean (±SD) AKT phosphorylation relative to control (set to 1.0) and the statistical significance of the indicated differences (Student's t-test).

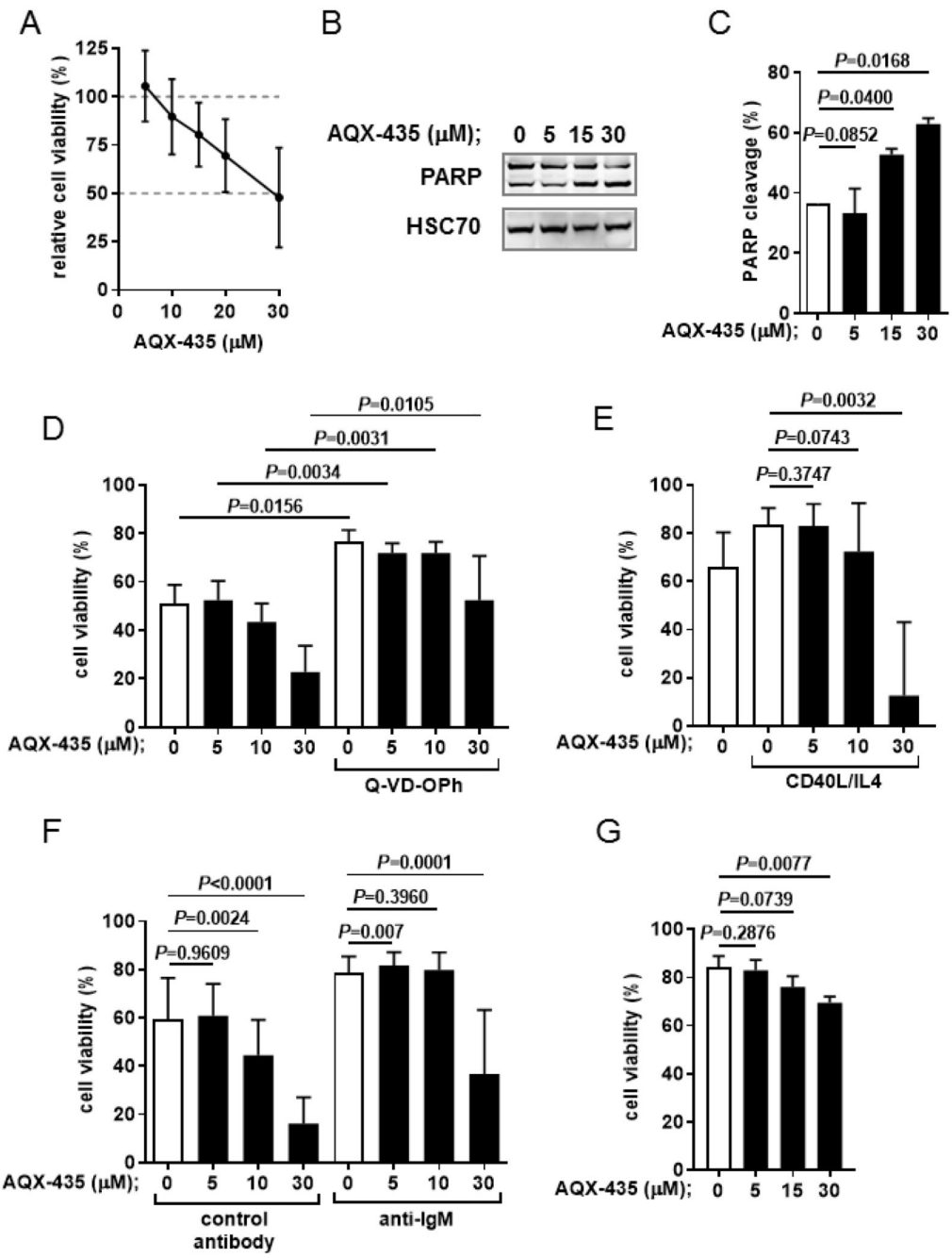

Figure 4.

AQX-435 induces caspase-dependent apoptosis of CLL cells and overcomes the survival promoting effects of microenvironment-related factors. **A,** CLL samples (n=24) were treated with various concentrations (5–30 μM) of AQX-435 or DMSO as a control for 24 hours and cell viability was analyzed using annexin V/PI staining. Graph shows mean (±SD) percentage of viable (annexin V^-/PI^-) cells. **B** and **C,** CLL samples were treated with the indicated concentrations of AQX-435 or DMSO as a control for 24 hours and PARP expression was analyzed by immunoblotting. **B,** Representative results and **C,** quantitation

for all samples analyzed (n=3). **D,** CLL samples (n=4) were incubated with the indicated concentrations of AQX-435 or DMSO in the presence or absence of Q-VD-OPh (10 μM). After 24 hours, cell viability was analyzed using annexin V/PI staining. **E** and **F,** CLL samples were incubated with the indicated concentrations of AQX-435 or DMSO in the presence or absence of **E,** CD40L/IL4 (n=10) or **F,** bead-bound anti-IgM or control antibody (n=9). After 24 hours, cell viability was analyzed using annexin V/PI staining. **G,** PBMCs from healthy donors (n=5) were treated with the indicated concentrations of AQX-435 or DMSO. After 24 hours, cells were stained with anti-CD19, anti-CD5, annexin V-FITC and PI and analyzed by flow cytometry. Graphs **C** to **G**, show mean (±SD) percentage of PARP cleavage or viable (annexin V^-/PI^-) cells and the statistical significance of the indicated differences (Student's t-test).

Europe PMC Funders Author Manuscripts

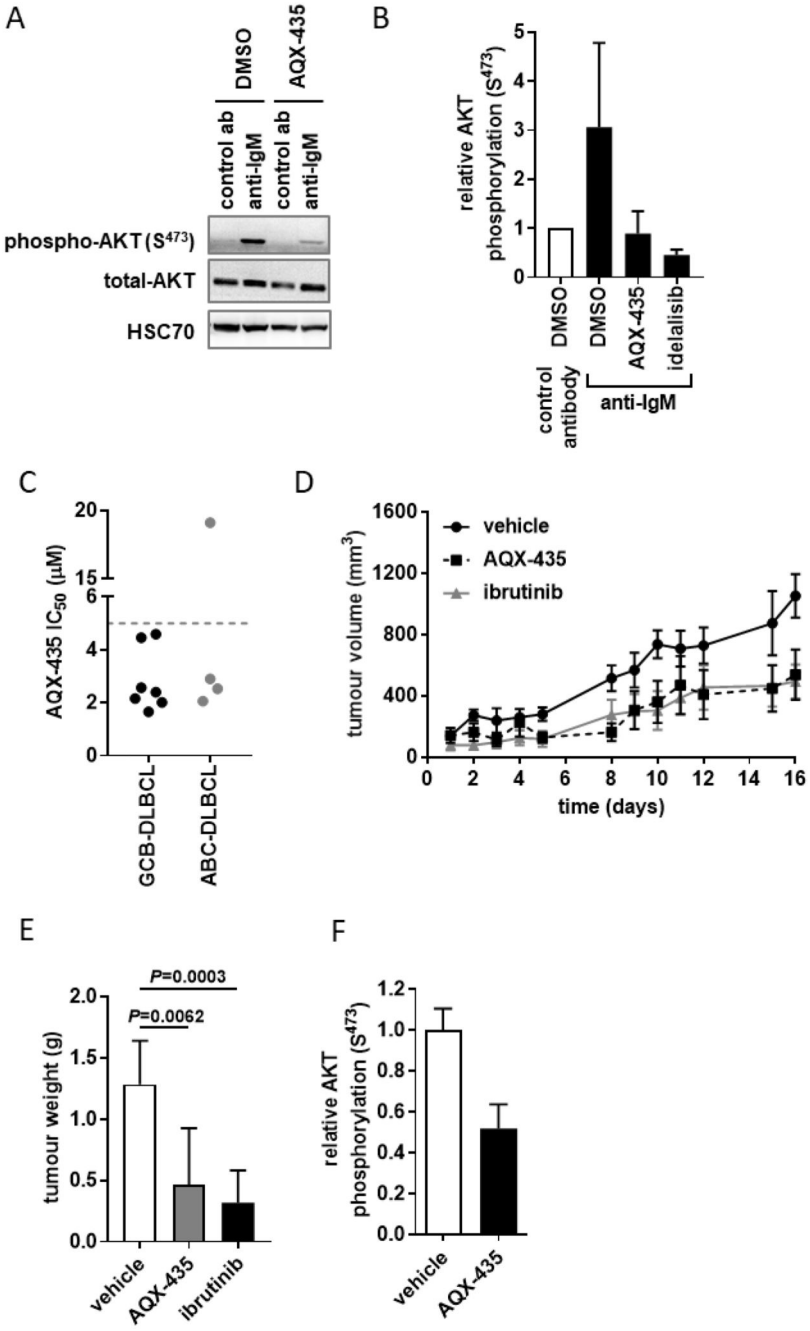

Figure 5.

Effects of AQX-435 on DLBCL cell lines in vitro and inhibition of AKT phosphorylation and tumor growth in TMD8 cells *in vivo*. **A** and **B,** TMD8 cells were pre-treated with AQX-435 (30 μM), idelalisib (1 μM) or DMSO for 30 minutes and then stimulated with soluble anti-IgM or control antibody (ab) for 15 minutes. Expression of total and phospho-AKT (S^{473}) was analyzed by immunoblotting. HSC70 was analyzed as an additional loading control. Figures show **A,** representative immunoblot (of n=9 experiments performed) and **B,** quantitation (mean ±SD) for direct comparison for AQX-435 and idelalisib in 4 individual

Europe PMC Funders Author Manuscripts

experiments. Graph shows mean (±SD) fold increase relative to control antibody/DMSO-treated cells (set to 1.0). **C,** Growth inhibitory activity of AQX-435 in a panel of GCB (WSU-DLCL2, SU-DHL-4, SU-DHL-5, SU-DHL-6, Toledo, OCI-LY19, KARPAS-422) and ABC-DLBCL (TMD8, U2932, HBL1, OCI-LY10) derived cell lines. IC_{50} values were determined using CellTitre Glo (Promega) in 96-well plates after 72 hours of drug exposure and using DMSO-treated cells as controls. **D** and **E,** Mice bearing TMD8 tumors were treated with AQX-435 (10 mg/kg) or vehicle control (both ip). Ibrutinib (25 mg/kg, po) was used as a positive control. Graphs shows **D,** mean (±SD) tumor volume at the indicated times following initiation of treatment and **E,** mean (±SD) tumor weight at the end of the experiment. The statistical significance of the indicated differences is shown (Student's t-test). **F,** Mean (±SD) AKT (S^{473}) phosphorylation in TMD8 tumors following ip administration of AQX-435 (10 mg/kg, n=2) or vehicle control (n=3) with values for vehicle control set to 1.0. Note we were unable to obtain intact protein from one tumor from the AQX-435-treated mice (see Supplementary Fig. 10C).

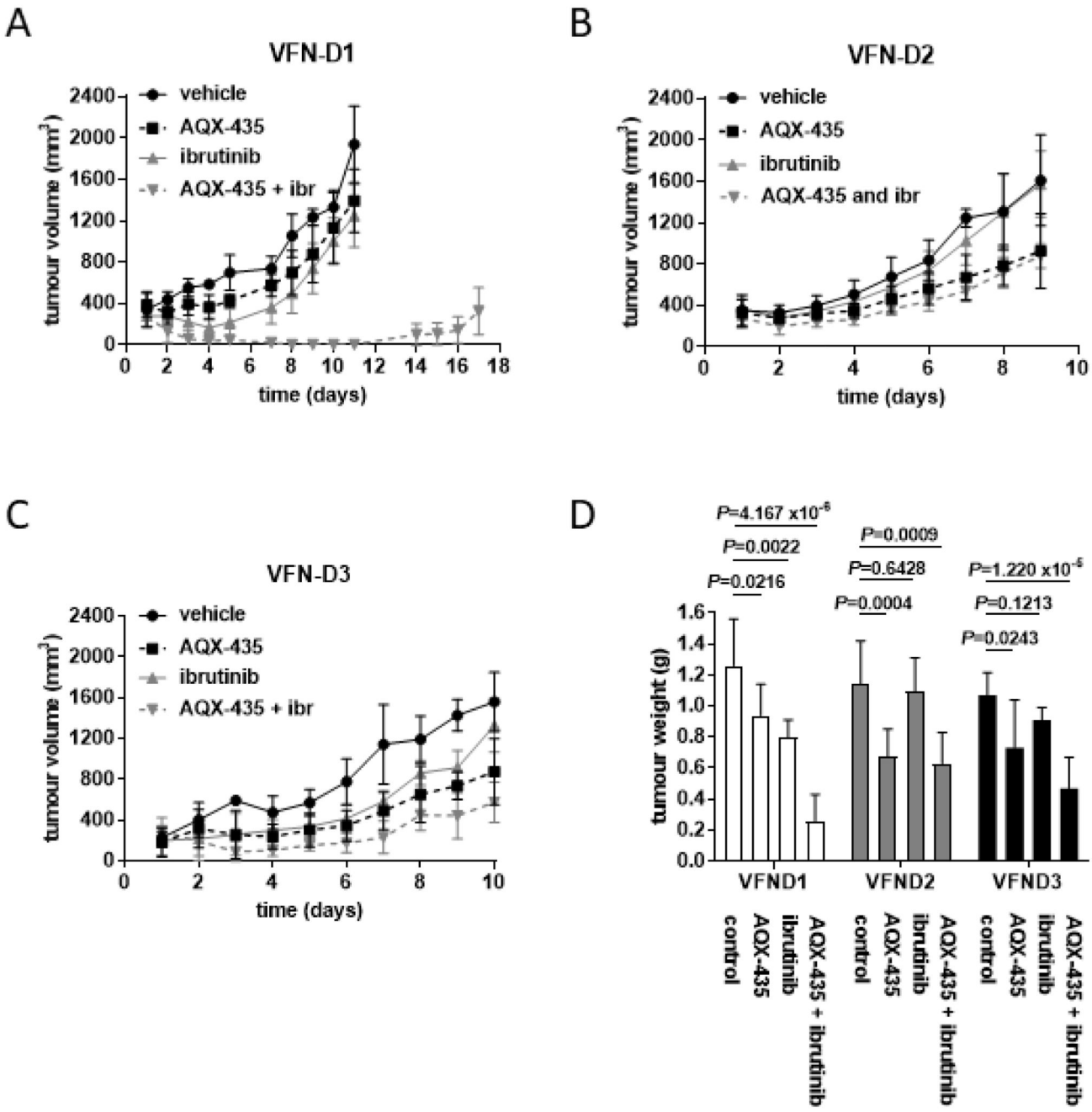

Figure 6.

Effects of combined treated with AQX-435 and ibrutinib in DLBCL PDX models. Mice bearing DLBCL PDX tumors (VFN-D1, D2 and D3) were treated with AQX-435 (50 mg/kg; ip), ibrutinib (25 mg/kg, po), the combination of AQX-435 and ibrutinib, or vehicle control. **A** to **C,** Mean (±SD) tumor volume at the indicated times following initiation of treatment. **D,** Mean tumor weight (±SD) at the end of the experiment with the statistical significant of the indicated differences (Student's t-test).